doi:10.3788/gzxb20174611.1125001

饱和模式下微通道板输出电子云的 Monte-Carlo 仿真

谢运涛,张玉钧,孙晓泉
(电子工程学院 脉冲功率激光技术国家重点实验室,合肥 230037)

摘 要:当基于微通道板(MCP)的光电探测器受到强辐射干扰时,MCP 的饱和将导致探测器的时间分辨率和空间分辨率发生改变.本文建立了饱和工作状态下 MCP 电子云运动仿真模型,与常规的线性工作状态的不同之处在于,该模型考虑了 MCP 通道壁上累积的正电荷对通道内电子云运动特性的影响.仿真结果表明,当 MCP 工作在线性状态,电极浸入深度的不同对通道电子云能量分布有很大差异,而工作在饱和状态,通道电子云能量分布趋于一致.电子能量分布曲线与相关文献的实验数据拟合良好,验证了模型的正确性.

关键词:微通道板;饱和;Monte Carlo;电子云;渡跃时间
中图分类号:TN144+.1; TN23 **文献标识码**:A **文章编号**:1004-4213(2017)11-1125001-9

Monte-Carlo Simulation of Output Electron Cloud from a Microchannel Plate in a Saturation Mode

XIE Yun-tao, ZHANG Yu-jun, SUN Xiao-quan
(*State Key Laboratory of Pulsed Power Laser Technology, Electronic Engineering Institute, Hefei* 230037, *China*)

Abstract: The performance of microchannel plate (MCP) detectors, including the temporal and spatial resolutions, varies significantly for MCPs work in a saturated mode due to high intensity illumination. In this paper, the influence of positive charges which accumulate on inner channel wall was added to a electron cloud motion model. It is the main difference between the MCP model in a saturated and a non-saturated mode. The kinetic characteristics of the electron clouds were calculated and analyzed. Simulation results show that the Energy Distributions Of Electrons (EDOEs), in a saturated mode, have a similar shape for MCPs with different electrode penetrate depth. This is very different from the results obtained in a non-saturated case. It is concluded that these phenomena come from the accumulation of positive charges near the exit of the channel. The EDOEs fit well with the experimental data of related literature, which verifies the correctness of this model.

Key words: Microchannel plate; Saturation; Monte Carlo; Electron cloud; Transit time
OCIS Codes: 250.0250; 260.7210; 040.7190; 120.4640

0 Introduction

Microchannel plate (MCP) has many advantages, such as high gain, high temporal resolution, and high spatial resolution et al.[1-2]. It is widely used in the detection of particles and photons, such as the UV image intensifier[3]. The image qualities, including the temporal and spatial resolutions, vary significantly while MCP detectors are illuminated with different intensities of lights[4]. There are lots of researches on

Foundation item: National Science Foundation for Young Scientists of China (No. 41605015); State KeyLaboratory of Pulsed Power Laser Technology Funds (No. SKL2016ZR06)
First author: XIE Yun-tao (1990—), male, Ph.D. degree, mainly focuses on the laser interference technology. Email: wsqijian@126.com
Supervisor(Contact author): SUN Xiao-quan (1962—), male, professor, Ph.D. degree, mainly focuses on optical technology. Email: sunxq@ustc.com
Received: Feb.20, 2017; **Accepted**: Jun.26, 2017

the performance of the MCPs irradiated with low-intensity light[3-4], but few researches on the performance of MCPs in high-intensity environment, such as in photoelectric counteraction.

Theoutput Energy Distribution Of Electrons (EDOE) and Angle Distribution Of Electrons (ADOE) have important influences on the image quality of MCP[5]. According to previous literatures, most of studies focus on the EDOE and ADOE for MCPs work in a linear mode. Chen L[6] got very close approximation of EDOE, but didn't discuss the ADOE. Price and Fraser[5] studied the ADOE and EDOE specifically, but the calculated curves only fit well with the experiment data at low energy. Yan L et al.[7] calculated the ADOE and EDOE of MCP, and got the MTF function of the MCP while it works in a linear mode. In summary, there are few reports about ADOE and EDOE of MCP in saturation mode(when MCP is irradiated with high intensity light).

Numerical method isa important way to study the avalanche process of electrons in MCP[8]. It means to track electrons with Monte Carlo method. This method could be used to study the MCP gain[9], transit time[4,10], EDOE and ADOE[5,7]. The main disadvantage of this method is the large amount of computation, especially for 3D models. Besides, professional programming skills are also required due to the problem of non-convergence when numerical method is used in characterizing real devices.

With theimprovement of computing power and the development of commercial software, simulations of the avalanche processes by numerical methods become feasible[4,10-11]. In this paper, we modeled the cascade process of the electrons in MCP by COMSOL Multiphysics. By comparing the transit time, EDOE and ADOE of the MCP between the non-saturated mode and the saturated mode, we got the characteristics of MCP with different geometries. Simulation results fit well with available experimental data, indicating that this model can be used in the analysis of the performance of MCP with different geometries in a saturated or non-saturated mode.

1 Model and method

1.1 Three-dimensional MCP model

MCP is a glass wafer consist of parallel array of millions of tiny electronic channels fused together with channel pore size in the range of 4-20 μm. Channels are arranged in a regular hexagonal structure[12], and length to diameter ratio is in the range of 40∶1 to 60∶1. The channel is coated with metal electrodes at its both ends, and the penetrate depth of the electrode is about 0.5 to 3 times the diameter of the channel. The channel material is lead silicate glass.

As for the actual MCPs, parameters of the 3D model are summarized in Table 1.

Table 1 Parameters in 3D model

Parameter	Value
Diameter/ μm	10
Length/μm	400
Bias angle/(°)	8
Dielectric constant[10]	6

In COMSOL Multiphysics, the 3D geometry of the microchannel plate is shown as Fig.1. Considering the mutual influence of the electric fields between adjacent channels, the adjacent six tubes should be taken into account to calculate the accelerating electric field generated by the voltage between the two electrodes.

Fig.2 shows the cross section of the MCP model in XOZ plane. Voltage between the photocathode and the entrance of MCP is 20 V and the primary electrons are accelerated in this field until they fly into the channel. The initial energy of primary electrons is 1 eV. The offset voltage across the MCP electrode is 1 000 V, which produces an accelerating electric field. The primary electrons are accelerated by the field to hit the channel wall, resulting in secondary electrons. Then the secondary electrons are accelerated and collide with the wall until they fly out of the channel.

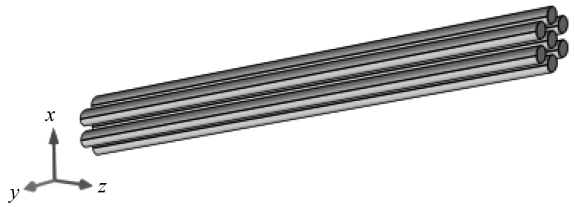

Fig.1 3D geometry of the MCP in COMSOL Multiphysics

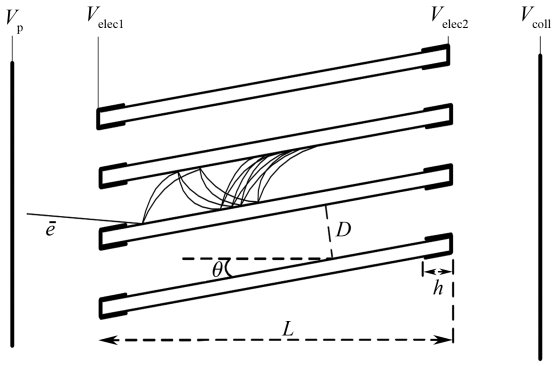

Fig.2 Cross section of the MCP

In MCP, each channel acts as an independent electron multiplier. The influence of the electron clouds in adjacent channels can be ignored. This simplification is reasonable and accord well with experimental results while MCPs run at low frequency or ultraviolet environment.

1.2 Secondary electron emission model

In this model, it is important to represent the electron emission process from the channel wall. The mean yield of secondary electrons is determined by the incident energy and incident angle of primary electrons. The incident energy $V_m(\theta_i)$, at which the incident electron colliding with the wall will produce the maximum secondary electron yield, can be expressed as follows[13]

$$V_m(\theta_i) = V_m(0)/\sqrt{\cos\theta_i} \tag{1}$$

where $V_m(0)$ is the energy of getting maximum yield while the electron incidents at normal angle, and θ_i is the incident angle. As for the lead silicon glass, $V_m(0)$ in the literature is in the range of 200～300 eV, in this model we set it to 270 eV.

The maximum yield of secondary electrons as a function of the incident angle of primary electron is givenas[13]

$$\delta_m(\theta_i) = \delta_m(0)\exp[\alpha(1-\cos\theta_i)] \tag{2}$$

where α is closely related to the channel material. As for the lead silicate glass, the value of α is between 0.4 and 0.6, so we set it to 0.5 in this model[8]. $\delta_m(0)$ represents the maximum yield while colliding at normal angle, which ranges from 3.0 to 4.0. We take it to be 4.0.

When primary electron incidents at angle θ_i and with energy V_i, the mean yield of secondary electron could be expressed as[13]

$$\delta(V_i,\delta_i) = \delta_m(\theta_i)\,\frac{\beta V_i/V_m(\theta_i)}{\beta-1+[V_i/V_m(\theta_i)]^\beta} \tag{3}$$

where β is a variable determined by the channel material. It must be bigger than 1 and its general value is 1.3[8].

The actual number of secondary electron is a random number assigned by sampling a Poisson distribution with a mean value of $\delta(V_i,\delta_i)$.

The initial energy of each secondary electron follows a Maxwell-Boltzmann probability distribution[13]

$$P(E_s) = C(E_s/E_0)\exp(-E_s/E_0) \tag{4}$$

where E_0 is the most probable energy. As for lead silicate glass, the typical value of E_0 is 2～3 eV and is taken to be 3 eV in this model[8]. C is the normalization constant.

The initial emission angle of each secondary electron is independent of the state of the primary electron. The azimuth angle ϕ is sampled from a uniform distribution with the range of 0 to 2π and the polar angle θ is sampled from a cosine distribution with the range of 0 to $\pi/2$.[13]

$$P(\theta) = \cos(\theta) \tag{5}$$

1.3 Tracking

In the 3D model, when the electron flies into the channel, it will be accelerated by electric field. So electron′s velocity $\boldsymbol{v}$ and displacement $\boldsymbol{s}$ are determined by the ballistic trajectory function as follows

$$\frac{\mathrm{d}}{\mathrm{d}t}[m\boldsymbol{v}(x,y,z)] = q\boldsymbol{E}(x,y,z) \tag{6}$$

$$\frac{\mathrm{d}\boldsymbol{s}(x,y,z)}{\mathrm{d}t}=\boldsymbol{v}(x,y,z) \tag{7}$$

where $\boldsymbol{E}$ is the electronic field.

In a non-saturated mode, the electronic field in the channel only comes from the voltage between the two electrodes. This built-in electric field can be calculated by the following formula

$$\boldsymbol{E}_1=-\nabla V \tag{8}$$

where V represents for the voltage between the two electrodes.

The penetrate depth of the electrode has a significant influence on the distribution of the built-in electric field. Fig.3 shows the calculated electric field while the penetrate depth to channel diameter ratio (h/D) is set to 1, $h/D=1$; $V_{\mathrm{p}}=-95$ V; $V_{\mathrm{elec1}}=-75$ V; $V_{\mathrm{elec2}}=-20$ V; $V_{\mathrm{coll}}=0$ V. It is clear that, the electric field in the electrode region is weaker than in other regions, and is not uniformly distributed. This type of distribution has the effect of decreasing the width of ADOE[14].

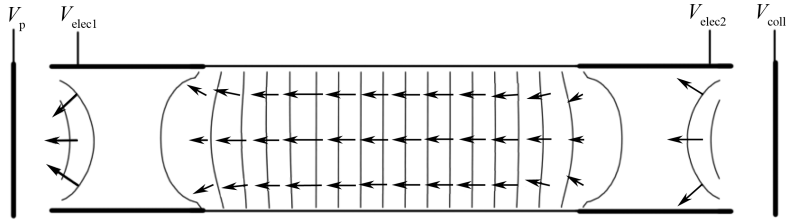

Fig.3 Equipotentials and electric field near the exit of channel

When MCP works in a saturated mode, the electric field generated by positive charges on the inner surface of the channel can't be ignored. According to the law of conservation of charge, positive charges accumulate for $N-1$ per secondary emission on the internal surface of the channel, where N is the yield of secondary electron. The electric field produced by positive charges could be calculated by Poisson equation

$$\nabla\cdot(\varepsilon_0\varepsilon_r\boldsymbol{E}_2)=\rho_s \tag{9}$$

where ρ_s represents for the total positive surface charge density. The total electric field in the channel is the sum of $\boldsymbol{E}_1$ and $\boldsymbol{E}_2$.

In order to calculate the electric field generated by the positive charges in COMSOL Multiphysics, first an accumulator need to be set to count the value of the total positive charges on the inner surface of the channel in charged particle tracing interface, and then the electrostatics interface is applied to calculate the field from the positive charges. The tolerance of the voltage was set to be 0.01 V when calculating the electric field. The maximum time step was 0.1 ps and the total calculation time was 200 ps when tracing the electrons.

2 Comparisons

2.1 Transit time

To analyze the effect of saturation on the kinetic characteristics of the electrons in the channel, we have carried out a lot of simulations with different number of incident electrons. In Fig. 4, we represent the variation of the number of output electrons with the number of incident electrons. When the incident electron is less than 20, the number of output electrons increases linearly with the number of input electrons, indicating that the gain of the channel is almost constant. However, when the incident electron is greater than 20, as the number of incident electrons increases, the gain begins to decrease gradually, which means the occurrence of gain saturation.

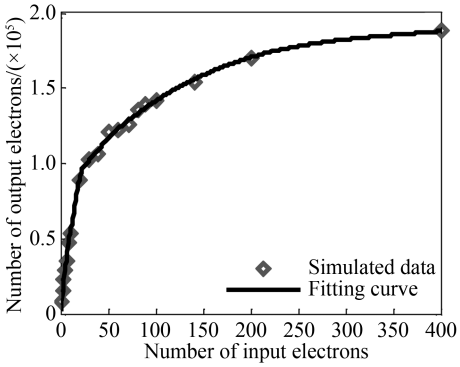

Fig.4 Variation of the number of output electrons with the number of incident electrons

Fig.5(a) and (b) show the positions of electron clouds at different time with 20 and 200 incident

particles, respectively. As we can see, the electron clouds move toward the channel exit along with the avalanche process. Once a small amount of particles are introduced at the entrance, there appears a large number of particles in the channel. It means that the channel has a very high gain. Compared with Fig.5 (b), the electron cloud in Fig.5(a) appears to be closer to the channel exit at the same time. This phenomenon is more pronounced in Fig.6.

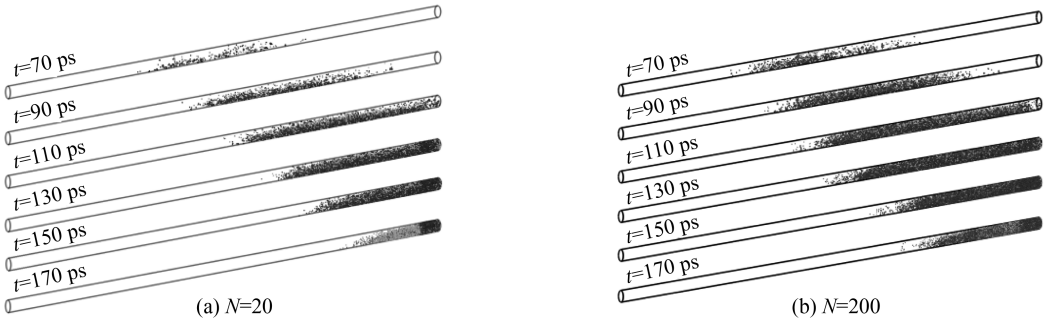

Fig.5 Evolution of spatial distribution of secondary electron cloud in channel

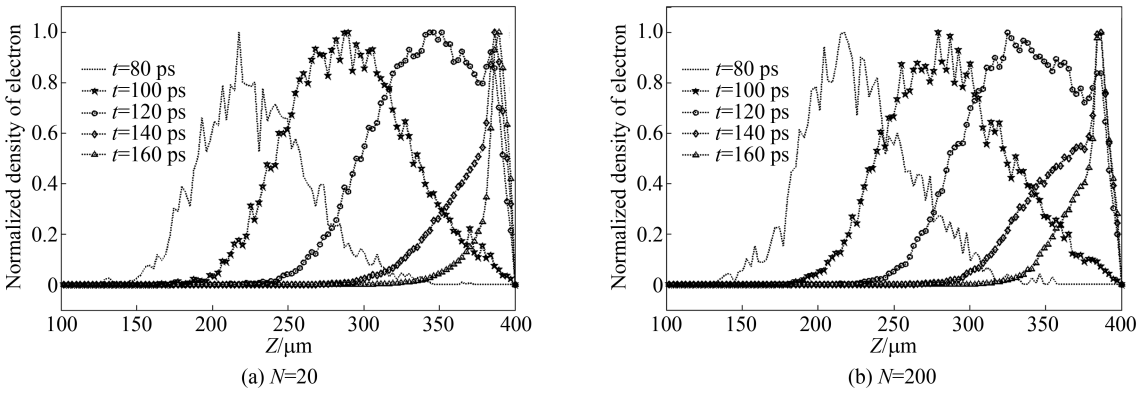

Fig.6 Normalized density of electron cloud along the axis of channel at different time

Fig.6 shows the electron density distributions along the channel axis at different time. The curves are cut off at 400 μm where some of the electrons have flown off the channel. When $t=120$ ps, the curves appear upturned at the area of 390 μm$<Z<$400 μm both in Fig.6(a) and Fig.6(b). It means the accumulation of electrons at the electrode area. Whereas, there are obvious difference between the curves at $t=140$ ps in Fig.6(a) and (b): the curve in Fig.6(b) is significantly higher than the curve in Fig.6(a) at the area of 350 μm$<Z<$390 μm. Similar phenomenon also appears at $t=160$ ps. It is concluded that in a saturated mode, the proportion of the electrons accumulated in front of the electrode area is much higher than that in a non-saturated mode.

Fig.7 shows the transit time distribution of the electrons with 20, 80, 140 and 200 electrons. We can see it clearly that these curves approximate the Gaussian distribution. The instant at which the output electron pulse reaches its peak amplitude is about 160 ps for different number of primary electrons, which is consistent with Ref. [4], indicating that the saturation effect has no significant influence on the transit time of the channel. But the saturation effect makes the transit time curve expand obviously. As the number of the input electrons increases, the full width at half maximum (FWHM) of these curves increases gradually. The FWHM of the curve with $N=20$ is 40 ps, while the FWHM of the curve with

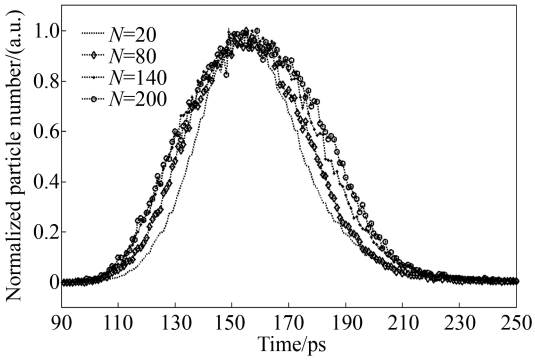

Fig.7 Transit time distribution of the output electrons with different number of primary electrons

$N=200$ becomes 60 ps. Therefore, more primary electrons will make the electron clouds more dispersed and will eventually reduce the time resolution of the MCP detectors.

2.2 EDOE

Koshida et al.[15] measured the EDOE as a function of incident current. It was found that the electrons with energy greater than 50 eV decrease significantly as the incident current increased. Price[5] also obtained similar results through simulations.

Fig.8 (c) shows the EDOE calculated in this paper. With the increase in the number of incident particle, the proportion of the emission electrons with energy between 10 eV to 30 eV increases, which is in good agreement with the conclusion in Ref.[15]. The variation of the proportion of electrons with different energy leads to the gradual disappearance of the sub-peak in EDOE.

Fig.8(b) shows the calculated data of Ref.[5]. Obviously, the results in the saturated mode agree well with experimental results[16-17] in Fig.8(a) at low energy, but the fit deviating at higher energy. In our calculation, curves in Fig.8(c) show very good fits whether at low energy or at high energy both in the saturated mode and non-saturated mode. The main difference between these two simulations is the method of calculating the influence of the saturation effect. In Ref.[5], the electric field generated by the wall charge is calculated by a empirical formula, but in this paper we use the Poisson formula.

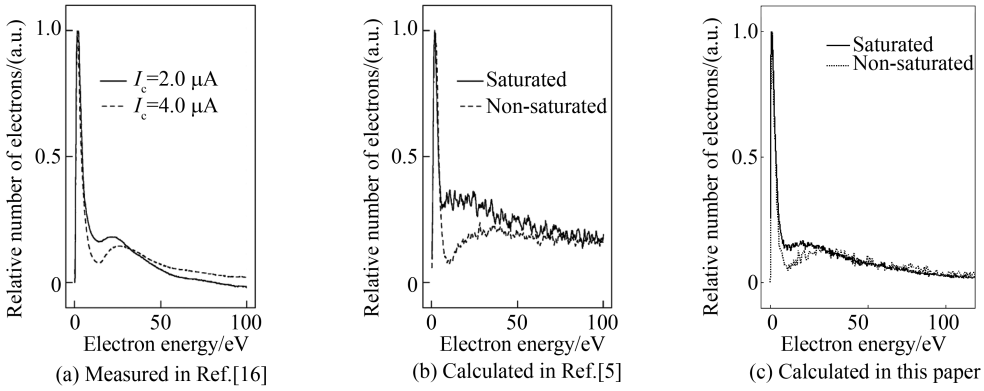

Fig.8 Calculated andmeasured EDOEs

In the case of linear gain, the penetrate depth of the electrode has a marked effect on the EDOE of the channel. Fig.9(a) shows the EDOE of the channels with different h to D ratio. We can see it clearly that the increase in the ratio helps to suppress the tail of the distribution and improve the monochromaticity of the output electrons. When ratio=0.5, ratio=1 and ratio=1.5, the EDOEs appear two obvious peaks. The main peak is at low energy, while the sub-peak is at high energy. Increasing the ratio significantly suppress the height of the sub-peak.

The EDOEs of the output electrons in a saturated mode are showed in Fig.9(b). The differences between the EDOEs with ratio=0.5, 1 and 1.5 reduced gradually. It means that the performances of the MCPs with different geometries trend to be converge when exposed to strong light.

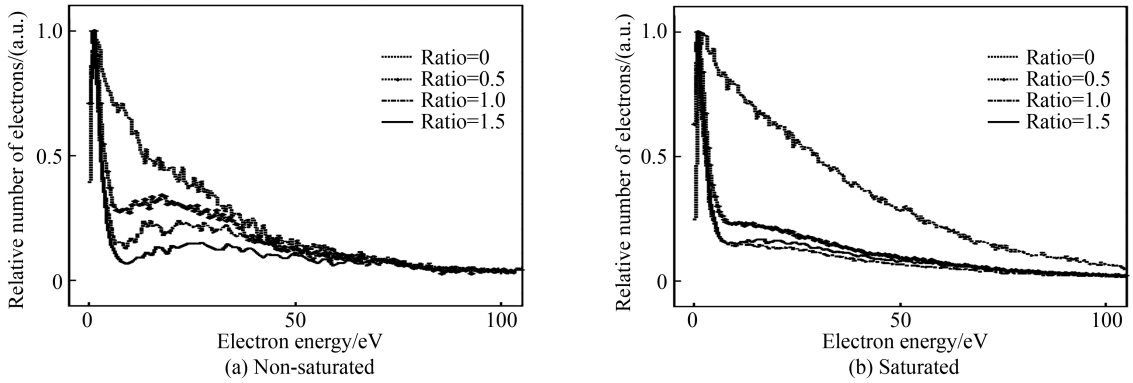

Fig.9 EDOEsfor channels with different h/D ratio

2.3 ADOE

In Ref.[18], Bronshteyn measured the ADOE and concluded that the FWHM of the ADOE curve is in the range of 5 to 15 degrees. In Fig.10(a), the FWHMs of the ADOEs in a non-saturated mode, which show no systematic variation with h/D, are about 10°. Our result is consistent with the data by Bronshteyn[17], but is larger than the data by Price[5], which is about 2°.

We also get the ADOEs of the channels with different h/D ratios in a saturated mode, as shown in Fig.10(b). We see that, the FWHMs of the ADOEs in a saturated mode are about 10 degrees, which show no significant difference with the results in the non-saturated mode. However, there are obvious differences between the ADOEs in Fig.10(a) and (b). The electron number reaches peak value at 8° in the saturated mode, while in the non-saturated mode the electron number reaches the peak value at 2°. It means that the emission electrons are more divergent in the saturated mode.

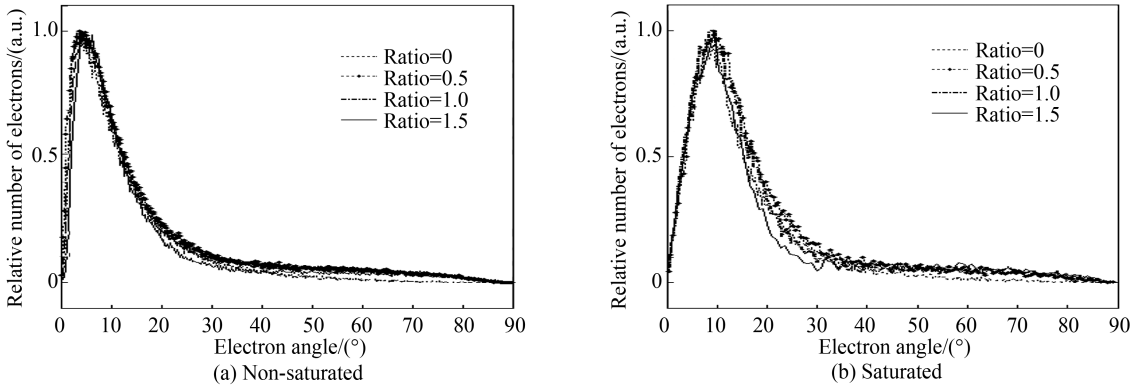

Fig.10 ADOEs for channels with different ratio

3 Discussions

As Fig.8(a) shows, the EDOE in a non-saturated mode has two peaks. The main peak with a sharp protuberance at low energy and the sub-peak with a very long tail at high energy. This characteristic of the EDOE primarily depends on the distribution of the electric field in the channel. As show in Fig.11, the channel is divided into two parts according to the distribution of the electric field: region A with a weaker electric field and region B with remarkable acceleration electric field. When MCPs work in a non-saturated mode, the output electrons come from both region A and region B, so there are two peaks in Fig.8(a). The electrons emitted from region A result in the main peak in the EDOE, while the sub-peak result from the electrons from region B.

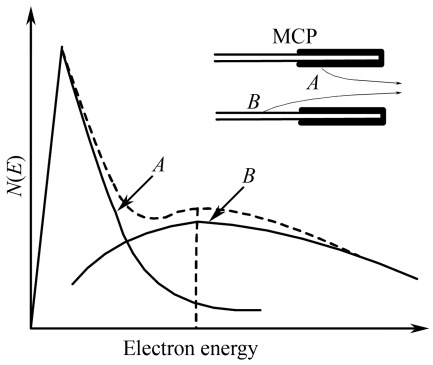

Fig.11 EDOE of electrons from different parts of the channel

With the large number of incident electron, the effect of the positive charges can not be neglected. Since the positive charge in region B changes the original electric field, which makes the electrons collide with the wall more frequently, shortening the electrons' accelerating distance and resulting in the suppression of the tail of the EDOE.

Simulation results validate thispoint. Fig.12 shows the evolution of positive charge distribution on the inner surface of the channel with 200 input particles from 110 ps to 180 ps. Along with the electronic avalanche process, the density of the positive charges in the channel increases sharply and finally reaches its maximum value at region B. When $t=140$ ps, the biggest positive surface charge density is only 1.4×10^{-3} C/m^2, but it sharply increases to 6.84×10^{-3} C/m^2 when $t=180$ ps.

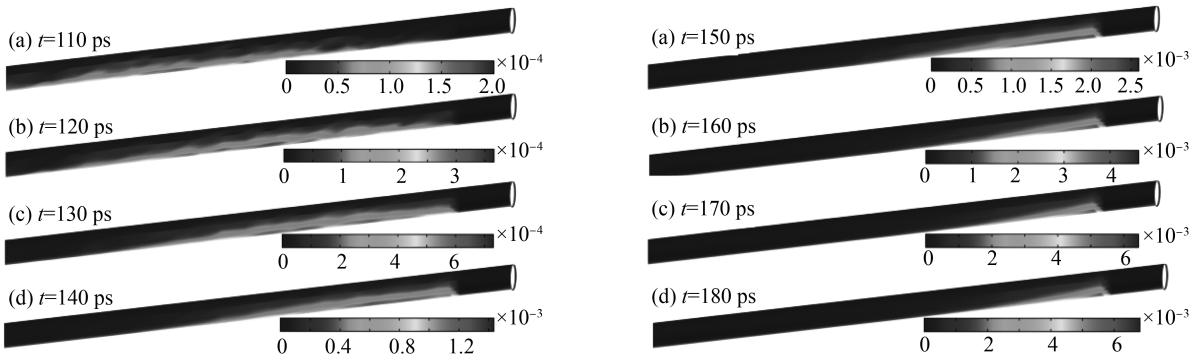

Fig.12 Evolution of the positive charge accumulatedat the inner surface of channel

Fig.13 presents the electronic field distribution near the exit of the channel at $t=180$ ps. It is easy to find that the maximum intensity of electric field in region B, about 4×10^6 V/m, is nearly 2 times of the intensity of the built-in electric field in this region, which is about 2.3×10^6 V/m. It is easy to conclude that the positive charge accumulated in the inner surface of the channel significantly change the electric field distribution in region B, and it also has a great influence in region A.

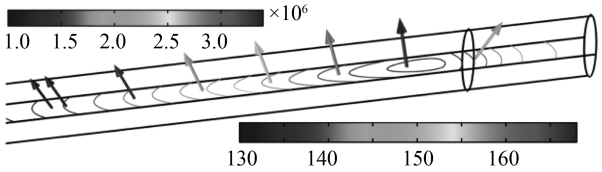

Fig. 13 Equipotentials and electronic field generated by positive charges at 180 ps

In region B, the electric field generated by the positive charge is perpendicular to the channel axis, which forces electrons to collide with the wall in advance and therefore shorten the distance for electrons to accelerate. It indicates that the proportion of the electrons with energy higher than 50 eV decreases obviously as the number of incident electrons increases[15]. In addition, the number of the secondary electron decreases with the energy reducing, which explains the gain saturation of the MCP. Compared with region B, region A is much closer to the channel exit. Electrons from region A are more divergent, which explains the angle dispersion of electron clouds in a saturation mode.

4 Conclusion

In this paper, we present a 3D model of MCP established in COMSOL Multiphysics, and calculate the influence of the wall charges on the electron clouds in the channel. The transit time, ADOE and EDOE of the output electron clouds are simulated and analyzed both in a saturated and non-saturated mode. In the saturated case, the accumulated positive charges on the inner surface of the channel significantly affect the electric field near the exit of the channel, and change the kinetic characteristic of the electron clouds. As a result, the angle of the output electron become divergent and the energy trend to concentrate in a narrow range at low energy. The reduction of the energy of the electron cloud further affects the gain of MCP, leading to gain saturation. These simulation results are in good agreement with the experimental data, indicating the effectiveness of this model.

References

[1] CAI H, LIU J, NIU L, *et al*. MCP gated x-ray framing camera[C]. International Conference on Optical Instrumentation and Technology. International Society for Optics and Photonics, 2009: 751327.

[2] CAO Zhu-rong, ZHANG Hai-ying, DONG Jian-jun, *et al*. High dynamic range imaging and application to laser-plasma diagnostics in inertial confinement fusion (ICF) experiment[J]. *Acta Physica Sinica*, 2011, **60**(4): 422-427.

[3] CHENG H, SHI F, FENG L, *et al*. Performance characteristics of solar blind UV image intensifier tube[C]. International Symposium on Photoelectronic Detection and Imaging. International Society for Optics and Photonics, 2009: 73840H.

[4] WANG Q, YUAN Z, CAO Z, *et al*. Three-dimensional particle-in-cell simulation on gain saturation effect of microchannel plate.[J]. *Review of Scientific Instruments*, 2016, **87**(7): 214-552.

[5] PRICE G J, FRASER G W. Calculation of the output charge cloud from a microchannel plate[J]. *Nuclear Instruments & Methods in Physics Research*, 2001, **474**(474): 188-196.

[6] CHEN L, WANG X, TIAN J, *et al*. Simulation of the effects of coated material SEY property on output electron energy

distribution and gain of microchannel plates[J]. *Nuclear Instruments and Methods in Physics Research Section A*, 2016, **840**: 133-138.

[7] YAN L, SHI F, CHENG H, *et al*. Monte Carlo simulation of electron transport in low-light-level image intensifier[J]. *Optik-International Journal for Light and Electron Optics*, 2015, **126**(2): 219-222.

[8] WU M, KRUSCHWITZ C A, MORGAN D V, *et al*. Monte Carlo simulations of microchannel plate detectors. I. Steady-state voltage bias results[J]. *Review of Scientific Instruments*, 2008, **79**(7): 073104.

[9] KRUSCHWITZ C A, WU M, ROCHAU G A. Monte Carlo simulations of microchannel plate detectors. II. Pulsed voltage results[J]. *Review of Scientific Instruments*, 2011, **82**(2): 023102.

[10] WANG Qiang-qiang, DENG Ke-li, DENG Cai-bo, *et al*. Three-dimensional numeric simulation of multiplication process of secondary electrons in microchannel plate[J]. *High Power Laser and Partical Beams*, 2015, **27**(12): 190-195.

[11] IVANOV V, INSEPOV Z, ANTIPOV S. Simulation of gain and timing resolution in saturated pores[J]. *Nuclear Instruments and Methods in Physics Research Section A*, 2011, **639**(639): 158-161.

[12] SIEGMUND O H W, TREMSIN A S, VALLERGA J V. Advanced MCP sensors for UV/visible astronomy and biology[J]. *Nuclear Instruments and Methods in Physics Research Section A*, 2003, **510**(1): 185-189.

[13] BRUINING H. Physics and applications of secondary electron emission: pergamon science series: electronics and waves—a series of monographs[M]. *Elsevier*, 2016.

[14] BAI Xiao-hong, ZHU Bing-li, XU Peng, *et al*. Simulating the spatial resolution of the framing camera[C]. SPIE, 2016, **10141**: 1014118-1.

[15] KOSHIDA N. Effects of electrode structure on output electron energy distribution of microchannel plates[J]. *Review of Scientific Instruments*, 1986, **57**(3): 354-358.

[16] KOSHIDA N, MIDORIKAWA M, KIUCHI Y. Output energy distribution of a microchannel plate[J]. *Advances in Electronics & Electron Physics*, 1985, **64**(149): 337-342.

[17] PAN Jing-sheng, GU Yan, SUN Jian-ning, *et al*. Thermal neutron sensitive MCPs for neutron radiograph[J]. *Optics and Precision Engineering*, 2015, **23**(3): 660-666.

[18] BRONSHTEYN I M, YEVDOKIMOV A V, TYUTIKOV A M, *et al*. Differential secondary emission characteristics of microchannel plates[J]. *Radio Engineering and Electronic Physics*, 1979, **24**(4): 871-874.